JACS JOURNAL OF THE AMERICAN CHEMICAL SOCIETY

Article

Cite This: J. Am. Chem. Soc. 2019, 141, 19935−19940

pubs.acs.org/JACS

Bis-Monophospholyl Dysprosium Cation Showing Magnetic Hysteresis at 48 K

Peter Evans, Daniel Reta, George F.S. Whitehead, Nicholas F. Chilton,* and David P. Mills*

Department of Chemistry, School of Natural Sciences, The University of Manchester, Oxford Road, Manchester M13 9PL, United Kingdom

Supporting Information

ABSTRACT: Single-molecule magnets (SMMs) have potential applications in high-density data storage, but magnetic relaxation times at elevated temperatures must be increased to make them practically useful. Bis-cyclopentadienyl lanthanide sandwich complexes have emerged as the leading candidates for SMMs that show magnetic memory at liquid nitrogen temperatures, but the relaxation mechanisms mediated by aromatic C_5 rings have not been fully established. Here we synthesize a bis-monophospholyl dysprosium SMM $[Dy(Dtp)_2][Al\{OC(CF_3)_3\}_4]$ (**1**, Dtp = $\{P(C^tBuCMe)_2\}$) by the treatment of *in-situ*-prepared "$[Dy(Dtp)_2(C_3H_5)]$" with $[HNEt_3][Al\{OC(CF_3)_3\}_4]$. SQUID magnetometry reveals that **1** has an effective barrier to magnetization reversal of 1760 K (1223 cm^{-1}) and magnetic hysteresis up to 48 K. *Ab initio* calculation of the spin dynamics reveals that transitions out of the ground state are slower in **1** than in the first reported dysprosocenium SMM, $[Dy(Cp^{ttt})_2][B(C_6F_5)_4]$ (Cp^{ttt} = $C_5H_2{}^tBu_3$-1,2,4); however, relaxation is faster in **1** overall due to the compression of electronic energies and to vibrational modes being brought on-resonance by the chemical and structural changes introduced by the bis-Dtp framework. With the preparation and analysis of **1**, we are thus able to further refine our understanding of relaxation processes operating in bis-C_5/C_4P sandwich lanthanide SMMs, which is the necessary first step toward rationally achieving higher magnetic blocking temperatures in these systems in the future.

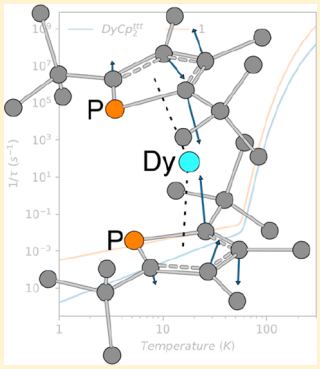

INTRODUCTION

The potential for high-density data storage devices based on single-molecule magnets (SMMs) is reliant upon increasing spin relaxation times toward practically useful time scales at relatively high temperatures, away from expensive liquid helium regimes to that of cheap and abundant liquid nitrogen.[1] Lanthanide (Ln) based SMMs have been at the forefront of research in this area for the past 15 years,[2] and design principles popularized by Rinehart and Long in 2011[3] directed the community toward longer relaxation times by means of massive increases in the energy barrier to magnetic reversal (U_{eff}).[4] These large increases in U_{eff} did not lead to corresponding increases in magnetic remanance temperatures[5] until the dysprosocenium cation $[Dy(Cp^{ttt})_2]^+$ (Cp^{ttt} = $C_5H_2tBu_3$-1,2,4) was shown to exhibit magnetic hysteresis at T_H = 60 K in 2017.[6] We attributed the high-temperature magnetic remanance in this bis-Cp^{ttt} system to the combination of a Dy^{3+} center with rigid, charge-dense π-aromatic rings; we also predicted that removal of C−H groups from the C_5 ring could increase hysteresis temperatures further.[6a] This has been proven correct, with hysteresis temperatures up to T_H = 80 K observed for peralkylated bis-cyclopentadienyl Ln complexes reported in the past two years.[7]

An alternative strategy to remove C−H groups from C_5 frameworks is heteroatom substitution;[8] indeed, the magnetic properties of theoretical $[Dy(E_5)_2]^+$ (E = N, P) cations have recently been predicted to exhibit high U_{eff} values.[9] Phospholyl ligands are a valid alternative to cyclopentadienyls as the P lone pairs are relatively soft, so they tend to exhibit η^5-binding modes with Ln ions.[10] Synthetic routes toward peralkylated monophospholyls are already mature; of most relevance here, the Ln chemistry of $\{P(C^tBuCMe)_2\}$ (Dtp) has already been developed.[11] The straightforward synthesis of $[Dy(Dtp)_2(I)]$ from DyI_3 and 2 equiv of KDtp was reported by Nief and co-workers in 2009,[11d] and we envisaged that this would be an ideal starting material toward the isolation of a $[Dy(Dtp)_2]^+$ cation. Herein we report the synthesis and magnetic properties of this cation and correlate our results with *ab initio* calculations of the spin dynamics to probe the effects of aromatic P−C vibrational modes in magnetic relaxation mechanisms compared to aromatic C−C vibrations. We find that relaxation is expedited in the $[Dy(Dtp)_2]^+$ cation compared to $[Dy(Cp^{ttt})_2]^+$ as additional vibrational modes are brought on-resonance, providing new insights into the relaxation pathways that operate in bis-C_4P vs bis-C_5 Ln sandwich SMMs.

RESULTS AND DISCUSSION

Synthesis. Treatment of "$[Dy(Dtp)_2(C_3H_5)]$" with $[NEt_3H][Al\{OC(CF_3)_3\}_4]$ in benzene gave $[Dy(Dtp)_2][Al\{OC(CF_3)_3\}_4]$ (**1**) following workup and recrystallization from chlorobenzene (Scheme 1). "$[Dy(Dtp)_2(C_3H_5)]$" was prepared from the salt metathesis reaction of $[Dy(Dtp)_2(I)]$[11d]

Received: October 25, 2019
Published: November 21, 2019

DOI: 10.1021/jacs.9b11515
J. Am. Chem. Soc. 2019, 141, 19935−19940

Scheme 1. Synthesis of 1

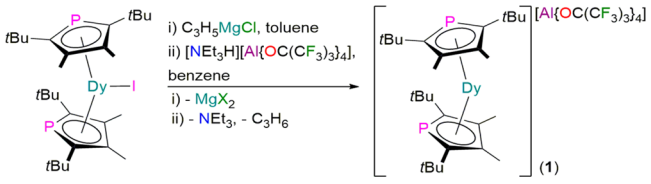

with C_3H_5MgCl, while $[NEt_3H][Al\{OC(CF_3)_3\}_4]$ was isolated from the reaction of $Li[Al\{OC(CF_3)_3\}_4]$[12] with NEt_3HCl by adapting procedures used for the synthesis of $[NEt_3H][B(C_6F_5)_4]$.[13] Crude "$[Dy(Dtp)_2(C_3H_5)]$" was obtained as an orange foam and was used *in situ* without further purification; we were unable to isolate the pure complex to collect meaningful characterization data due to its high solubility in pentane, but we are confident of its formulation from the formation of **1**. The global yield of **1** is 26% over three reaction steps based on DyI_3. The triethylammonium reagent was selected as it provides an entropic driving force with dual amine and alkene elimination during the reaction,[14] and the $[Al\{OC(CF_3)_3\}_4]^-$ anion is more weakly coordinating than the $[B(C_6F_5)_4]^-$ anion,[15] which has been used for the synthesis of all Ln metallocenium cations to date.[6,7,16] The direct reaction of $[Dy(Dtp)_2(I)]$ with $[H(SiEt_3)_2][B(C_6F_5)_4]$[17] gave an intractable mixture of products. ^1H, ^{13}C, and ^{31}P NMR spectra of a sample of **1** in d_5-chlorobenzene were uninformative due to paramagnetism, but the $[Al\{OC(CF_3)_3\}_4]^-$ anion was detected by ^{19}F NMR spectroscopy (δ_F: −90.50 ppm; $\nu_{1/2}$ = 300 Hz); the presence of paramagnetic $[Dy(Dtp)_2]^+$ cations has broadened this signal and shifted it considerably from the $[NEt_3H][Al\{OC(CF_3)_3\}_4]$ precursor (δ_F: −75.70 ppm, d_2-DCM).

Structural Characterization. The solid-state structure of **1** was determined by single-crystal X-ray diffraction (Figure 1). The $[Dy(Dtp)_2]^+$ cation in **1** exhibits a bent geometry, with a $Dtp_{cent}\cdots Dy\cdots Dtp_{cent}$ angle of 157.94(4)° and mean $Dy\cdots Dtp_{cent}$ distances of 2.354(3) Å; although this is slightly less

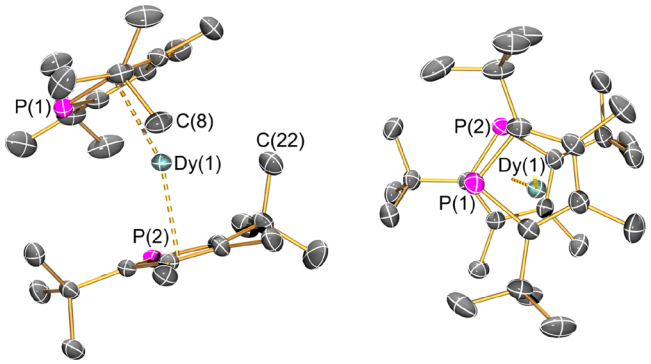

Figure 1. Molecular structure of the cation of $[Dy(Dtp)_2][Al\{OC(CF_3)_3\}_4]$ (**1**) with selected atom labeling: left, side view; right, top view. Displacement ellipsoids are set at the 50% probability level, and the anion and hydrogen atoms are omitted for clarity. Dy atoms are teal. P atoms are purple, and C atoms are gray. Selected bond distances (Å) and angles (deg): $Dy(1)\cdots Dtp_{cent}(1)$, 2.355(2); $Dy(1)\cdots Dtp_{cent}(2)$, 2.352(2); Dy(1)···P(1), 2.7981(8); Dy(1)···P(2), 2.7880(8); range $Dy(1)\cdots C_{Dtp}$, 2.570(3)−2.780(3); Dy(1)···C(8), 2.881(3); Dy(1)···C(22), 3.026(4); Dy(1)···H(8A), 2.481; Dy(1)···H(22A), 2.541; $Dtp_{cent}(1)\cdots Dy(1)\cdots Dtp_{cent}(2)$, 157.94(4); C(8)···Dy(1)···C(22), 115.38(9).

bent than $[Dy(Cp^{ttt})_2][B(C_6F_5)_4]$ ($Cp^{ttt}_{cent}\cdots Dy\cdots Cp^{ttt}_{cent}$, 152.56(7)°; $Dy\cdots Cp^{ttt}_{cent}$, 2.316(3) Å),[6a] the incorporation of phosphorus in the rings has led to increased Dy−ligand distances. As expected from removal of an equatorial iodide, the Dy^{3+} center in **1** has a larger $Dtp_{cent}\cdots Dy\cdots Dtp_{cent}$ angle and shorter $Dy\cdots Dtp_{cent}$ distances than the precursor $[Dy(Dtp)_2(I)]$ ($Dtp_{cent}\cdots Dy\cdots Dtp_{cent}$, 147.29(3)°; mean $Dy\cdots Dtp_{cent}$, 2.416(2) Å).[11d] The Dtp rings in **1** are staggered with respect to each other, with the phosphorus atoms at adjacent positions (mean Dy−P, 2.7931(11) Å). Although an η^5-binding mode is adopted, there is a significant variation in $Dy-C_{Dtp}$ distances: range 2.570(3)−2.780(3) Å, *cf.*, 2.702(2)−2.778(2) Å for $[Dy(Dtp)_2(I)]$.[11d] The electron deficient Dy^{3+} center in **1** forms additional stabilizing electrostatic contacts with ^{t}Bu groups, with two short Dy···C (2.881(3) and 3.026(4) Å) and two short Dy···H (2.481 and 2.541 Å) distances; similar metrical parameters for electrostatic interactions between Dy^{3+} centers and two C−H bonds of ^{t}Bu groups were previously seen for $[Dy(Cp^{ttt})_2][B(C_6F_5)_4]$ (Dy···C, 2.964(5) Å mean; Dy···H, 2.4989 Å mean).[6a] The metrical parameters of the $[Al\{OC(CF_3)_3\}_4]^-$ anions are unremarkable, and these do not show any interaction with the Dy^{3+} center (shortest Dy···F distance >6.0 Å).

Magnetism. A polycrystalline sample of **1** suspended in eicosane was analyzed by SQUID magnetometry to determine its magnetic properties. The magnetic susceptibility temperature product ($\chi_M T$) of solid **1** at 300 K is 13.85 cm^3 K mol^{-1} (Supporting Information Figure S8); this is in accord with the free-ion Curie value of 14.17 cm^3 K mol^{-1}[18] and *ab initio* calculations (13.66 cm^3 K mol^{-1}, see below). A steady reduction in $\chi_M T$ with temperature for solid **1** was observed down to 25 K (12.28 cm^3 K mol^{-1}), owing to thermal depopulation of the excited crystal field (CF) states. A more severe drop in $\chi_M T$ was observed below 25 K due to the onset of magnetic blocking, which correlates with the temperature at which the zero-field cooled (ZFC) susceptibility has a plateau (T_{B1} = 25 K; Figure S10). The nontraditional profiles of the field cooled (FC) and ZFC susceptibilities are a complicated function of the measurement protocol (temperature sweep rate, magnetic field strength, and field sweep rate) as well as the intricate field and temperature dependence of magnetic relaxation in Dy^{3+} SMMs;[19] such traces have been explained by others.[20] The most salient information from the FC/ZFC traces is the temperature at which the two data sets bifurcate: for **1**, T_{irrev} = 54 K (Figure S11).

Slow relaxation of magnetization for **1** was confirmed by the presence of out-of-phase maxima between 60 and 80 K in the zero-field ac susceptibility data (Figures S12 and S13). The temperature dependence of the relaxation times obtained from these measurements were fitted to a generalized Debye model using CC-FIT2[21] (Figure 2), which allows the extraction of uncertainties in the magnetic relaxation times from the underlying distribution function. We observe an exponential relaxation process (Orbach mechanism; $\tau^{-1} = \tau_0^{-1} \exp[-U_{eff}/T]$) above 50 K and extract an effective barrier to magnetization reversal U_{eff} = 1760(70) K (1220(50) cm^{-1}), with $\tau_0 = 10^{-11.7(4)}$ s (*ca.* 2 × 10^{-12} s). The U_{eff} value for **1** is identical to that previously seen for $[Dy(Cp^{ttt})_2][B(C_6F_5)_4]$ (1760 K),[6a] and smaller than the current record-holder $[Dy(C_5{}^iPr_5)(C_5Me_5)][B(C_6F_5)_4]$ (2217 K).[7b] To obtain relaxation times at lower temperatures, we performed magnetization decay experiments and fitted the data with stretched exponentials (Figure S14 and Table S3). Following a similar

DOI: 10.1021/jacs.9b11515
J. Am. Chem. Soc. 2019, 141, 19935−19940

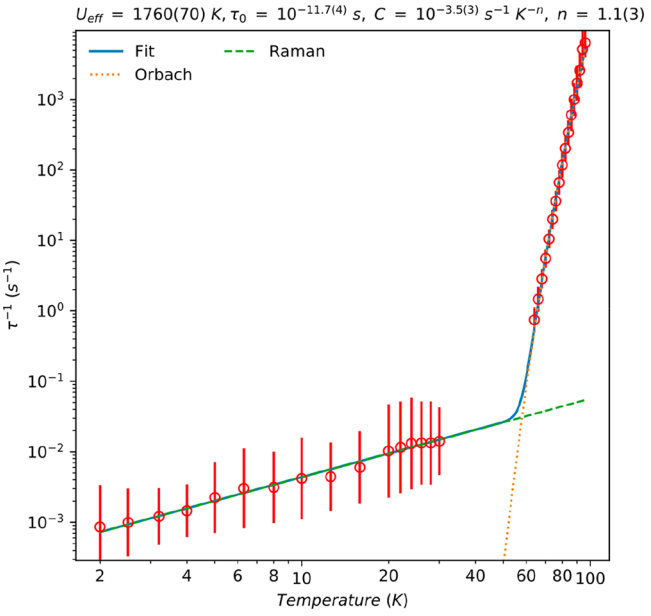

Figure 2. Temperature dependence of the magnetic relaxation rate of **1**. Red circles are the relaxation rates extracted from ac susceptibility data (high temperature) and dc magnetization decay data (low temperature); solid red lines are error bars from the distributions of relaxation times (see Supporting Information).[21] The solid blue line is given by $\tau^{-1} = \tau_0^{-1} \exp[-U_{eff}/T] + CT^n$. The dashed green line is given by $\tau^{-1} = \tau_0^{-1} \exp[-U_{eff}/T]$, and the dotted orange line is given by $\tau^{-1} = CT^n$ with U_{eff} = 1760(70) K, $\tau_0 = 10^{-11.7(4)}$ s, $C = 10^{-3.5(3)}$ s^{-1} K^{-n}, and n = 1.1(3).

approach for obtaining uncertainties from ac data,[21] we determined uncertainties from the magnetization decay experiments based on the well-known distribution underlying the stretched exponential function (see Supporting Information, Figure S14);[22] this gives $\tau_{\pm} = \tau_{\mu}\, e^{\pm 1.64 \tan[\frac{\pi}{2}(1-\beta)]/(1-\beta)^{0.141}}$ at the 1σ level, where β is the stretch factor. Below 30 K we observe a power-law relaxation process (Raman-like mechanism; $\tau^{-1} = CT^n$) for **1**, and this data is well-reproduced with n = 1.1(3) and $C = 10^{-3.5(3)}$ s^{-1} K^{-n} (*ca.* 3×10^{-4} s^{-1} K^{-n}). The small n value approaches that expected for the direct relaxation process;[23] however, as these data are collected in zero magnetic field, this is not a plausible mechanism. Indeed, all bis-cyclopentadienyl Dy^{3+} cations have relatively low Raman exponents of between 2 and 3 in the crystalline phase,[6,7] and thus, substitution of C for P in the first coordination sphere of **1** does not appear to grossly alter this characteristic; however, it cannot be ascertained if the even lower exponent of 1.1(3) here is due to the effect of the ring substitution or to the different counterion ($[Al\{OC(CF_3)_3\}_4]^-$, cf., $[B(C_6F_5)_4]^-$ for all dysprosocenium SMMs to date). While we cannot measure the relaxation dynamics between 30 and 64 K, extrapolation of the Orbach and Raman regions suggests that they intersect at 52 K which coincides with the bifurcation of FC/ZFC plots (T_{irrev} = 54 K): such a sharp intersection between the Raman and Orbach regions was observed for $[Dy(Cp^{ttt})_2][B(C_6F_5)_4]$, as was the coincidence of the intersection temperature and T_{irrev}.[6a] Using magnetization decays we have been able to directly measure the 100 s blocking temperature as T_{B2} = 23 K. Overall, magnetic relaxation is around 10−100 times faster in the range 2−100 K for **1** than for $[Dy(Cp^{ttt})_2][B(C_6F_5)_4]$ (Figure S15).

Solid **1** shows open, but comparatively waist-restricted, magnetic hysteresis loops up to T_H = 48 K (Figure 3), using a sweep rate of *ca.* 20 Oe/s around the important zero-field region where quantum tunneling of the magnetization (QTM) dominates for Ln SMMs.[4] The value of T_H for **1** is lower than the majority of isolated dysprosocenium cations reported to date, which have shown T_H values of 60−80 K,[6,7] except for one example, $[Dy(C_5{}^iPr_4H)_2][B(C_6F_5)]$ (T_H = 32 K),[7a] which contains ring C−H protons that have been postulated to enhance magnetic relaxation mechanisms.[6a] Despite the lack of ring protons in **1**, it shows open hysteresis to a maximum temperature that is 12 K lower than that previously seen for $[Dy(Cp^{ttt})_2][B(C_6F_5)_4]$ (T_H = 60 K).[6]

***Ab Initio* Calculations.** First-principles complete active space self-consistent field spin−orbit (CASSCF-SO) calculations were performed on the crystal structure of the cation in **1** to complement experimental data and to probe magnetic relaxation mechanisms (Table S4). As expected for a strongly

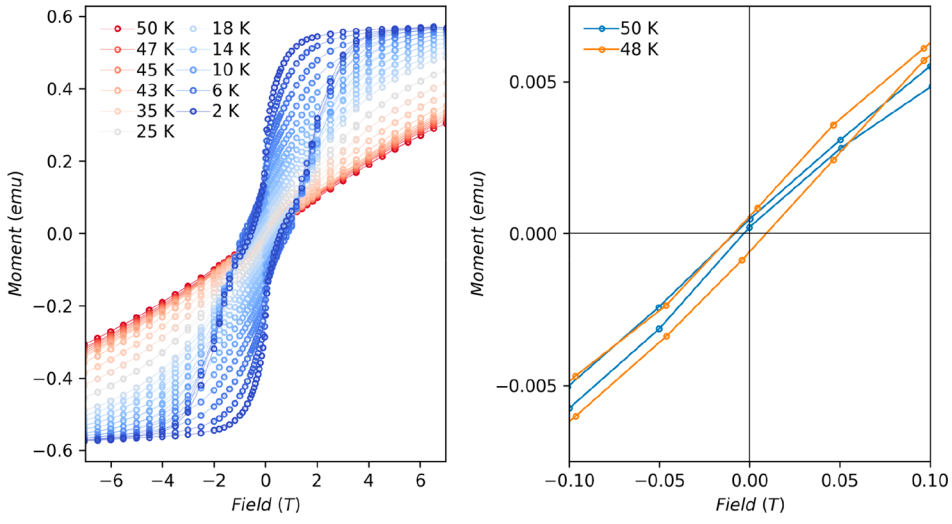

Figure 3. Magnetic hysteresis of solid **1**, measured with a mean field sweep rate of 21(9) Oe s^{-1} for $|H|$ < 10 kOe, 49(12) Oe s^{-1} for 10 < $|H|$ < 20 kOe, and 88(17) Oe s^{-1} for 20 < $|H|$ < 70 kOe. Hysteresis loops recorded from 2 to 18 K in 2 K steps, from 20 to 40 K in 5 K steps, and from 43 to 50 K in 1 K steps.

DOI: 10.1021/jacs.9b11515
J. Am. Chem. Soc. 2019, 141, 19935−19940

axial CF, we observe an easy-axis ground Kramers doublet corresponding to the $m_J = \pm 15/2$ CF state, where the first five excited states are also easy-axis-like and collinear with the ground doublet; the five excited states are dominated by $m_J = \pm 13/2$, $\pm 11/2$, $\pm 9/2$, $\pm 7/2$, and $\pm 5/2$, respectively. The *g*-values for the sixth excited Kramers doublet are highly rhombic, indicating a substantially mixed m_J composition, and thus magnetic relaxation by the Orbach process is likely to occur via this state (*ca.* 1716 K, which compares reasonably well with the experimental U_{eff} = 1760(70) K). To gain more insight into the relaxation dynamics, we have calculated the spin dynamics using our previously described *ab initio* method;[6a] briefly, this entails the following: (i) optimization of molecular geometry and determination of vibrational modes with DFT, (ii) calculation of spin−phonon coupling with CASSCF-SO, and (iii) simulation of magnetic relaxation via a semiclassical master equation (see Supporting Information for details). We find excellent agreement with the experimental data in the high-temperature region corresponding to Orbach relaxation (Figure 4a); note that relaxation via two-phonon Raman processes at low temperatures is not accounted for in these calculations. Examining the calculated relaxation rates carefully, we observe that relaxation shows two different exponential processes in different temperature regimes (Figure S17), and that this has a slight dependence upon the choice of phonon line width (Table S7). We find that magnetic relaxation follows an Orbach process over an effective barrier of *ca.* 1600−1700 K following the pathway shown in Figure 4b, but at temperatures less than *ca.* 52 K the effective barrier is reduced to *ca.* 660−960 K (Table S7 and Figures S17 and S18). The experimental data for **1** show only one Orbach process with U_{eff} = 1760(70) K down to 64 K and the onset of Raman relaxation below 30 K. Thus, a potential crossover to a smaller U_{eff} regime may occur between 64 and 30 K; however, we cannot probe these time scales with our instrumentation.

Decomposing the relaxation rates for the large U_{eff} process, the first step in magnetic relaxation is delicately balanced between the $|\pm 15/2\rangle$ to $|\pm 13/2\rangle$ and the $|\pm 15/2\rangle$ to $|\pm 11/2\rangle$ transitions: lower temperatures and larger phonon line widths favor the former, while higher temperatures and smaller phonon line widths favor the latter (Figure 4b, *cf.*, Figure S19). The $|\pm 15/2\rangle$ to $|\pm 13/2\rangle$ transition is mostly driven by mode 61, which is an in-plane deformation of the rings (Figure S20), whereas the $|\pm 15/2\rangle$ to $|\pm 11/2\rangle$ transition is driven by modes 76 and 77, which involve in-phase and out-of-phase deformations of the Dy^{3+} center via the carbon atoms of the Dtp rings (Figure S21).

Experimentally we observe that **1** relaxes faster than $[Dy(Cp^{ttt})_2][B(C_6F_5)_4]$ in the Orbach regime (Figure S15), and this is also borne out in comparable simulations (Figure S22; note that we have repeated calculations for $[Dy(Cp^{ttt})_2][B(C_6F_5)_4]$ using the slightly revised methodology employed here, see Table S6 and Figure S16). Seemingly in contradiction with the overall calculated relaxation rates (Figure S22), the escape rate of the $|\pm 15/2\rangle$ state in $[Dy(Cp^{ttt})_2][B(C_6F_5)_4]$ between 50 and 300 K is approximately an order of magnitude faster than that for **1** (Table S8), owing to the much faster $|\pm 15/2\rangle$ to $|\pm 13/2\rangle$ transitions in $[Dy(Cp^{ttt})_2][B(C_6F_5)_4]$ (Table S9). However, we note that all electronic states in **1** are compressed in energy, *cf.*, $[Dy(Cp^{ttt})_2][B(C_6F_5)_4]$ (Figure S23), due to a weaker crystal field, and that this brings the subsequent steps in relaxation ($|\pm 13/2\rangle$ to $|\pm 11/2\rangle$ at 229 cm^{-1}, $|\pm 11/2\rangle$ to $|\pm 9/2\rangle$ at 151 cm^{-1}, and $|\pm 9/2\rangle$ to $|\pm 7/2\rangle$ at 130 cm^{-1} for **1**) into resonance with vibrational modes with significant spin−phonon coupling (Figures S24 and S25 and Table S10). These excitations are 267, 172, and 157 cm^{-1} for $[Dy(Cp^{ttt})_2][B(C_6F_5)_4]$, and the relevant vibrational modes are further off-resonance (Figures S24 and S25). Therefore, although chemical alteration of the aromatic rings has made the initial steps in magnetic relaxation slower, confirming our hypothesis,[6a] magnetic relaxation in the Orbach regime in **1** is more efficient than for $[Dy(Cp^{ttt})_2][B(C_6F_5)_4]$ due to faster relaxation in the upper energy states of the manifold (Table S10).

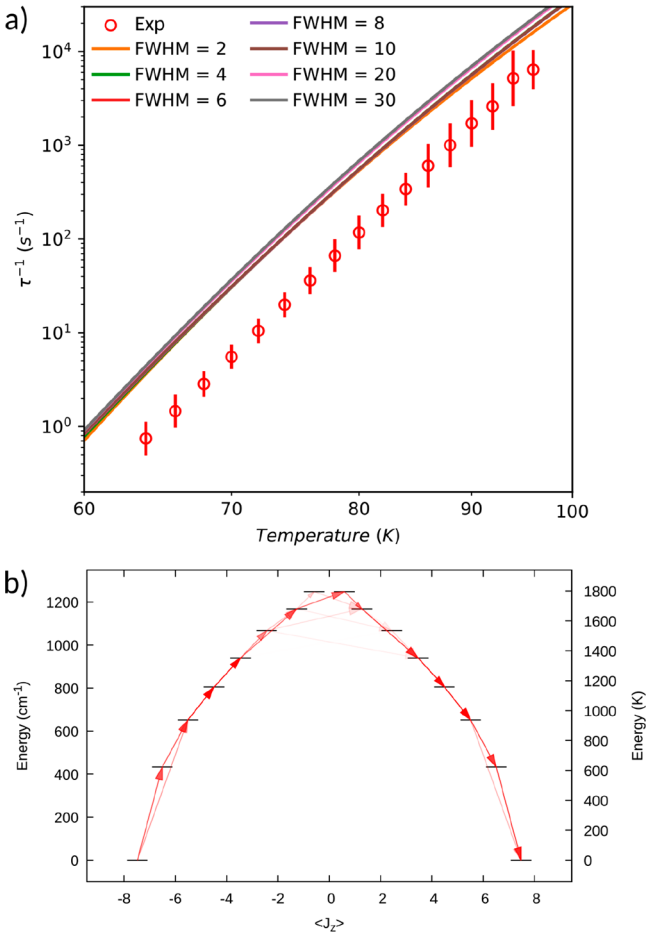

Figure 4. (a) *Ab initio* calculated magnetic relaxation rates for **1** (lines) compared with the experimental data (points). (b) Energy barrier to magnetic relaxation for **1**, calculated at 100 K and using a phonon linewidth of 6 cm^{-1}. Electronic states from CASSCF-SO calculations, decomposed in the J = 15/2 basis. The opacity of the arrows is proportional to the single-phonon transition probability normalized from each departing state and commencing with unit population in $|-15/2\rangle$; only relaxation pathways toward $|+15/2\rangle$ are shown. $\langle J_z \rangle$ is the expectation value of the J_z operator along the quantization axis.

CONCLUSION

In conclusion, we have shown that isolated bis-monophospholyl dysprosium cations can show relatively high U_{eff} and T_{max} values, in common with the cationic bis-cyclopentadienyl dysprosium family. Despite the lack of ring protons in $[Dy(Dtp)_2][Al\{OC(CF_3)_3\}_4]$, and its effective magnetization barrier being identical to that of $[Dy(Cp^{ttt})_2][B(C_6F_5)_4]$,[6a] the maximum hysteresis temperature of [Dy-

DOI: 10.1021/jacs.9b11515
J. Am. Chem. Soc. 2019, 141, 19935−19940

$(Dtp)_2][Al\{OC(CF_3)_3\}_4]$ is 12 K lower than this literature example. *Ab initio* calculations indicate that the replacement of aromatic C_5 rings with C_4P analogues has slowed down transitions out of the ground $|\pm 15/2\rangle$ doublet as intended. However, smaller energy gaps between excited states that are on-resonance with a series of vibrational modes have rendered relaxation more efficient overall in $[Dy(Dtp)_2][Al\{OC(CF_3)_3\}_4]$. Therefore, as with the bis-cyclopentadienyl dysprosium cation family,[6,7] the efficacy of magnetic relaxation processes in isolated bis-phospholyl dysprosium cations is also not trivially predictable. This is crucial new information for the future design of lanthanide SMMs with higher magnetic blocking temperatures.

EXPERIMENTAL SECTION

Materials and Methods. All manipulations were conducted under argon with the strict exclusion of oxygen and water by using Schlenk line and glovebox techniques. Benzene was dried by refluxing over potassium and was stored over a potassium mirror. Chlorobenzene was dried over CaH_2 and was stored over 4 Å molecular sieves. All solvents were degassed before use. For NMR spectroscopy, C_6D_5Cl was dried by refluxing over CaH_2 and was vacuum transferred and degassed by three freeze−pump−thaw cycles before use. $[Dy(Dtp)_2(I)]$[11d] and $Li[Al\{OC(CF_3)_3\}_4]$[12] were prepared according to literature methods, and DyI_3 (Alfa Aesar) and C_3H_5MgCl (Sigma-Aldrich) were purchased and were used as received. ^1H (400 MHz), ^{13}C (100 and 125 MHz), ^{31}P (162 MHz), and ^{19}F (376 MHz) NMR spectra were obtained on an Avance III 400 or 500 MHz spectrometer at 298 K. These were referenced to the solvent used or to external TMS (^1H, ^{13}C), H_3PO_4 (^{31}P), or $C_7H_5F_3$/$CDCl_3$ (^{19}F). FTIR spectra were recorded as microcrystalline powders using a Bruker Tensor 27 ATR-Fourier transform infrared (ATR-FTIR) spectrometer. Elemental analysis was carried out by Mr. Martin Jennings and Mrs. Anne Davies at the Microanalytical Service, School of Chemistry, University of Manchester.

Synthesis. *$[Dy(Dtp)_2][Al\{OC(CF_3)_3\}_4]$ (**1**).* A slurry of DyI_3 (0.4997 g, 0.92 mmol) and DtpK (0.5311 g, 2.02 mmol) in toluene (20 mL) was heated under reflux for 48 h. The resultant yellow reaction mixture was allowed to cool to room temperature and filtered; the remaining solids were washed with toluene (20 mL). A solution of $(C_3H_5)MgCl$ in THF (2.0 M, 0.7 mL, 1.4 mmol) was added to the yellow filtrate and stirred for 1.5 h to give an orange reaction mixture. The solvents were removed *in vacuo* to give a sticky orange solid, which was triturated with a mixture of *n*-hexane and dioxane (20:1, 30 mL). The product was extracted into *n*-hexane (15 mL) and filtered, and solvents were removed *in vacuo* to give an orange foam (0.4100 g, 0.63 mmol, 69% crude yield of the putative "$[Dy(Dtp)_2(C_3H_5)]$"). $[NEt_3H][Al\{OC(CF_3)_3\}_4]$ (0.6741 g, 0.63 mmol) and benzene (15 mL) were added, and the yellow-orange reaction mixture was stirred overnight. Volatiles from the resultant orange oil and yellow solution were removed *in vacuo*. The yellow foam obtained was washed with *n*-hexane (20 mL) and benzene (15 mL), and the residual solvent was removed *in vacuo* to give a yellow foam. The product was extracted into chlorobenzene (15 mL), filtered, and reduced in volume to 10 mL, and then layered with *n*-hexane (35 mL). After the reaction mixture was left standing for 3 days at room temperature, large yellow crystalswere obtained; these were washed with *n*-hexane and dried to give **1** (0.3764 g, 26% global yield based on DyI_3). Anal. Calcd (%) for $C_{44}H_{48}AlDyF_{36}O_4P_2$: C, 33.51; H, 3.07. Found: C, 30.86; H, 2.78. Elemental analysis results consistently gave lower carbon values than predicted, which we attribute to carbide formation from incomplete combustion. However, all other analytical data obtained are consistent with the bulk purity of **1**. χT product = 14.28 $cm^3\ mol^{-1}\ K$ (Evans method). ^{19}F NMR (C_6D_5Cl): $\delta = -90.50$ (br, $\nu_{1/2}$ = 300 Hz). The paramagnetism of **1** precluded assignment of its ^1H, ^{13}C, and ^{31}P NMR spectra. FTIR (ATR, microcrystalline; st = strong): $\tilde{\nu}$ = 2964 (w, br), 1472 (w), 1397 (w), 1352 (w), 1297 (m), 1274 (m), 1239 (m), 1210 (st), 1165 (m), 1022 (w), 970 (st), 832 (w, br), 726 (st), 660 (w), 624 (w), 560 (w), 536 (m), 442 (m) cm^{-1}.

$[NEt_3H][Al\{OC(CF_3)_3\}_4]$. A slurry of $Li[Al\{OC(CF_3)_3\}_4]$ (9.7404 g, 10.0 mmol) and NEt_3HCl (1.3765 g, 10.0 mmol) in DCM (175 mL) was stirred overnight. The resultant colorless suspension was filtered, and the solvent was removed from the filtrate *in vacuo* to give a white powder (7.3038 g, 68%). This was used without further purification; on one occasion the product was recrystallized from a saturated DCM solution and stored overnight at −35 °C, and the solid-state structure was determined by single-crystal XRD (see Supporting Information). Anal. Calcd (%) for $C_{22}H_{16}AlF_{36}N$: C, 24.71; H, 1.51; N, 1.31. Found: 24.71; H, 1.47; N, 1.46. ^1H NMR (CD_2Cl_2): δ = 1.44 (t, J_{HH} = 7.3 Hz, 9H, NCH_2CH_3), 3.3 (q, J_{HH} = 7.3 Hz, 6H, NCH_2CH_3), 4.92 (t, J_{NH} = 54 Hz, 1H, NH). ^{13}C NMR (CD_2Cl_2): δ = 9.45 (m, NCH_2CH_3), 49.04 (NCH_2CH_3), 78.75 (br, s, $OC(CF_3)_2$), 121.22 (q, J_{CF} = 293 Hz). ^{19}F NMR (CD_2Cl_2): $\delta = -75.70$. FTIR (ATR, microcrystalline): $\tilde{\nu}$ = 3252 (w), 2986 (w, br), 1746 (w), 1397 (w), 1353 (w), 1271 (s), 1240 (st), 1200 (m), 1024 (w), 967 (st), 833 (w), 797 (w), 756 (w), 725 (st, s), 561 (m), 536 (m), 439 (m) cm^{-1}.

ASSOCIATED CONTENT

Supporting Information

The Supporting Information is available free of charge at https://pubs.acs.org/doi/10.1021/jacs.9b11515.

Additional experimental details and results including crystallography and spectroscopy (PDF)

AUTHOR INFORMATION

Corresponding Authors

*nicholas.chilton@manchester.ac.uk
*david.mills@manchester.ac.uk

ORCID

Daniel Reta: 0000-0003-0000-9892
George F.S. Whitehead: 0000-0003-1949-4250
Nicholas F. Chilton: 0000-0002-8604-0171
David P. Mills: 0000-0003-1575-7754

Notes

The authors declare no competing financial interest.
Research data files supporting this publication are available from Mendeley Data at DOI: 10.17632/m4ssv5mxrz.1.

ACKNOWLEDGMENTS

We thank the UK Engineering and Physical Sciences Research Council (EPSRC) (EP/R002605X/1 for P.E., EP/P002560/1 for D.R. and EP/K039547/1 for a single-crystal X-ray diffractometer), and N.F.C. thanks the University of Manchester for a Presidential Fellowship and the Royal Society for a University Research Fellowship. We acknowledge the EPSRC UK National Electron Paramagnetic Resonance Service for access to the SQUID magnetometer, and the University of Manchester for access to the Computational Shared Facility.

REFERENCES

(1) Gatteschi, D.; Sessoli, R.; Villain, J. *Molecular Nanomagnets*; Oxford University Press, 2006.
(2) Ishikawa, N.; Sugita, M.; Ishikawa, T.; Koshihara, S.; Kaizu, Y. Lanthanide Double-Decker Complexes Functioning as Magnets at the Single-Molecular Level. *J. Am. Chem. Soc.* **2003**, *125*, 8694−8695.
(3) Rinehart, J. D.; Long, J. R. Exploiting single-ion anisotropy in the design of f-element single-molecule magnets. *Chem. Sci.* **2011**, *2*, 2078−2085.
(4) Layfield, R. A.; Murugesu, M. *Lanthanides and Actinides in Molecular Magnetism*; Wiley-VCH, 2015.

DOI: 10.1021/jacs.9b11515
J. Am. Chem. Soc. 2019, 141, 19935−19940

(5) Ding, Y.-S.; Chilton, N. F.; Winpenny, R. E. P.; Zheng, Y.-Z. On Approaching the Limit of Molecular Magnetic Anisotropy: A Near-Perfect Pentagonal BipyramidalDysprosium(III) Single-Molecule Magnet. *Angew. Chem., Int. Ed.* **2016**, *55*, 16071−16074.
(6) (a) Goodwin, C. A. P.; Ortu, F.; Reta, D.; Chilton, N. F.; Mills, D. P. Molecular magnetic hysteresis at 60 K in dysprosocenium. *Nature* **2017**, *548*, 439−442. (b) Guo, F.-S.; Day, B. M.; Chen, Y.-C.; Tong, M.-L.; Mansikkamäki, A.; Layfield, R. A. A dysprosium metallocene single-molecule magnet functioning at the axial limit. *Angew. Chem., Int. Ed.* **2017**, *56*, 11445−11449.
(7) (a) McClain, K. R.; Gould, C. A.; Chakarawet, K.; Teat, S. J.; Groshens, T. J.; Long, J. R.; Harvey, B. G. High-temperature magnetic blocking and magneto-structural correlations in a series of dysprosium(iii) metallocenium single-molecule magnets. *Chem. Sci.* **2018**, *9*, 8492−8503. (b) Guo, F.-S.; Day, B. M.; Chen, Y.-C.; Tong, M.-L.; Mansikkamäki, A.; Layfield, R. A. Magnetic hysteresis up to 80 K in a dysprosium metallocene single-molecule magnet. *Science* **2018**, *362*, 1400−1403. (c) Gould, C. A.; McClain, K. R.; Yu, J.; Groshens, T. J.; Furche, F.; Long, J. R.; Harvey, B. G. Synthesis and Magnetism of Neutral, Linear Metallocene Complexes of Terbium(II) and Dysprosium(II). *J. Am. Chem. Soc.* **2019**, *141*, 12967−12973.
(8) Guo, F.-S.; Bar, A. K.; Layfield, R. A. Main Group Chemistry at the Interface with Molecular Magnetism. *Chem. Rev.* **2019**, *119*, 8479−8505.
(9) Kotrle, K.; Herchel, R. Are Inorganic Single-Molecule Magnets a Possibility? A Theoretical Insight into Dysprosium Double-Deckers with Inorganic Ring Systems. *Inorg. Chem.* **2019**, *58*, 14046−14057.
(10) (a) Nief, F. Complexes containing bonds between group 3, lanthanide or actinide metals and non-first-row main group elements (excluding halogens). *Coord. Chem. Rev.* **1998**, *178*−*180*, 13−81. (b) Nief, F. Heterocyclopentadienyl Complexes of Group-3 Metals. *Eur. J. Inorg. Chem.* **2001**, *2001*, 891−904. (c) Le Floch, P. Phosphaalkene, phospholyl and phosphinine ligands: New tools in coordination chemistry and catalysis. *Coord. Chem. Rev.* **2006**, *250*, 627−681.
(11) (a) Nief, F.; Turcitu, D.; Ricard, L. Synthesis and structure of phospholyl- and arsolylthulium(ii) complexes. *Chem. Commun.* **2002**, 1646−1647. (b) Nief, F.; Turcitu, D.; Ricard, L. Structure and Reactivity of HomolepticSamarium(II) and Thulium(II) Phospholyl Complexes. *Chem. - Eur. J.* **2003**, *9*, 4916−4923. (c) Jaroschik, F.; Nief, F.; Le Goff, X.-F.; Ricard, F. Synthesis and Reactivity of Organometallic Complexes of Divalent Thulium with Cyclopentadienyl and Phospholyl Ligands. *Organometallics* **2007**, *26*, 3552−3558. (d) Jaroschik, F.; Nief, F.; Le Goff, X.-F. Sterically hindered cyclopentadienyl and phospholyl ligands in dysprosium chemistry. *Polyhedron* **2009**, *28*, 2744−2748. (e) Jacquot, L.; Xémard, M.; Clavaguéra, C.; Nocton, G. Multiple One-Electron Transfers in Bipyridine Complexes of Bis(phospholyl) Thulium. *Organometallics* **2014**, *33*, 4100−4106. (f) Jaroschik, F.; Momin, A.; Martinez, A.; Harakat, D.; Ricard, L.; Le Goff, X.-F.; Nocton, G. Synthesis and Characterization of 1,1′-Diphosphaplumbocenes: Oxidative Ligand Transfer Reactions with Divalent Thulium Complexes. *Organometallics* **2016**, *35*, 2032−2038.
(12) Krossing, I. The Facile Preparation of Weakly Coordinating Anions: Structure and Characterisation of Silverpolyfluoroalkoxyaluminates $AgAl(OR_F)_4$, Calculation of the Alkoxide Ion Affinity. *Chem. - Eur. J.* **2001**, *7*, 490−502.
(13) Uraguchi, D.; Kinoshita, N.; Kizu, T.; Ooi, T. Synergistic Catalysis of Ionic Brønsted Acid and Photosensitizer for a Redox Neutral Asymmetric α-Coupling of N-Arylaminomethanes with Aldimines. *J. Am. Chem. Soc.* **2015**, *137*, 13768−13771.
(14) Evans, W. J.; Seibel, C. A.; Ziller, J. W. Unsolvated Lanthanide Metallocene Cations $[(C_5Me_5)_2Ln][BPh_4]$: Multiple Syntheses, Structural Characterization, and Reactivity Including the Formation of $(C_5Me_5)_3Nd$. *J. Am. Chem. Soc.* **1998**, *120*, 6745−6752.
(15) Krossing, I.; Raabe, I. Noncoordinating Anions − Fact or Fiction? A Survey of Likely Candidates. *Angew. Chem., Int. Ed.* **2004**, *43*, 2066−2090.
(16) (a) Goodwin, C. A. P.; Reta, D.; Ortu, F.; Chilton, N. F.; Mills, D. P. Synthesis and Electronic Structures of Heavy Lanthanide Metallocenium Cations. *J. Am. Chem. Soc.* **2017**, *139*, 18714−18724. (b) Goodwin, C. A. P.; Reta, D.; Ortu, F.; Liu, J.; Chilton, N. F.; Mills, D. P. Terbocenium: completing a heavy lanthanide metallocenium cation family with an alternative anion abstraction strategy. *Chem. Commun.* **2018**, *54*, 9182−9185. (c) Liu, J.; Reta, D.; Cleghorn, J.; Yeoh, Y. X.; Ortu, F.; Goodwin, C. A. P.; Chilton, N. F.; Mills, D. P. Light Lanthanide Metallocenium Cations Exhibiting Weak Equatorial Anion Interactions. *Chem. - Eur. J.* **2019**, *25*, 7749−7758.
(17) Lambert, J. B.; Lin, L.; Keinan, S. The $C_5SiMe_7^+$ cation: pyramidal, bicyclic, or cyclohexadienyl? *Org. Biomol. Chem.* **2003**, *1*, 2559−2565.
(18) Atwood, D. A. *The Rare Earth Elements: Fundamentals and Applications*; John Wiley and Sons Ltd., 2012.
(19) Ding, Y.-S.; Yu, K.-X.; Reta, D.; Ortu, F.; Winpenny, R. E. P.; Zheng, Y.-Z.; Chilton, N. F. Field- and temperature-dependent quantum tunnelling of the magnetisation in a large barrier single-molecule magnet. *Nat. Commun.* **2018**, *9*, 3134.
(20) Liu, J.-L.; Chen, Y.-C.; Tong, M.-L. Symmetry strategies for high performance lanthanide-based single-molecule magnets. *Chem. Soc. Rev.* **2018**, *47*, 2431−2453.
(21) Reta, D.; Chilton, N. F. Uncertainty estimates for magnetic relaxation times and magnetic relaxation parameters. *Phys. Chem. Chem. Phys.* **2019**, *21*, 23567−23575.
(22) Johnston, D. C. Stretched exponential relaxation arising from a continuous sum of exponential decay. *Phys. Rev. B: Condens. Matter Mater. Phys.* **2006**, *74*, 184430.
(23) Abragam, A.; Bleaney, B. *Electron Paramagnetic Resonance of Transition Ions*; Clarendon Press: Oxford, 1970.

DOI: 10.1021/jacs.9b11515
J. Am. Chem. Soc. 2019, 141, 19935−19940